



Research articles

Evolution of structure and magnetic properties in $\text{Eu}_x\text{Bi}_{1-x}\text{FeO}_3$ multiferroics obtained under high pressure



I.I. Makoed^{a,*}, A.A. Amirov^{b,c}, N.A. Liedienov^{d,e,*}, A.V. Pashchenko^{d,e}, K.I. Yanushkevich^f,
D.V. Yakimchuk^f, E.Yu. Kaniukov^{g,h,i}

^a A.S. Pushkin Brest State University, 224016 Brest, Belarus

^b Institute of Physics, Dagestan Scientific Center of Russian Academy of Sciences, 367003 Makhachkala, Russia

^c Laboratory of Novel Magnetic Materials & Institute of Physics Mathematics and Informational Technologies, Immanuel Kant Baltic Federal University, 236029 Kaliningrad, Russia

^d State Key Laboratory of Superhard Materials, International Centre of Future Science of Jilin University, 130012 Changchun, China

^e Donetsk Institute for Physics and Engineering named after O.O. Galkin, NASU, 03028 Kyiv, Ukraine

^f Scientific-Practical Materials Research Center, NASB, 220072 Minsk, Belarus

^g Department of Electronic Materials Technology, National University of Science and Technology MISiS, 119049 Moscow, Russia

^h Laboratory of Single Crystal Growth, South Ural State University, 454080 Chelyabinsk, Russia

ⁱ The State Scientific Institution "The Institute of Chemistry of New Materials of National Academy of Sciences of Belarus", 220141 Minsk, Belarus

ARTICLE INFO

Keywords:

Multiferroics
Magnetocaloric effect
Néel temperature
Entropy
Heat capacity
Phase transition

ABSTRACT

The structure, microstructure, magnetic properties and magnetocaloric effect in the BiFeO_3 -based multiferroics with a partial isovalent substitution of bismuth for europium ions have been experimentally and theoretically investigated by X-ray diffraction, SEM and magnetic methods. The ceramic $\text{Eu}_x\text{Bi}_{1-x}\text{FeO}_3$ ($0 \leq x \leq 0.2$) samples have been prepared by a solid-state reaction method under cold pressing at high pressure $P = 4$ GPa. With increase in the concentration of the doping Eu element a structural phase transition from a rhombohedral $R3c$ to an orthorhombic $Pn21a$ perovskite structure is observed. Microstructure and chemical composition of the $\text{Eu}_x\text{Bi}_{1-x}\text{FeO}_3$ samples have been studied by SEM data. Temperature dependences of magnetization for the Eu-doped multiferroics demonstrate two magnetic “weak ferromagnetic-antiferromagnetic” and “antiferromagnetic-paramagnetic” phase transitions in a high temperature range $T = 640\text{--}822$ K. The presence of a weak ferromagnetism in all compositions is confirmed by open loops of magnetic field dependencies. On the basis of the analysis of magnetic data, magnetic entropy change, heat capacity change, relative cooling power and full-width at half-maximum of the peak have been calculated. It has been found out that the thermodynamic characteristics strongly depend on the degree of substitution, temperature, and magnitude of magnetic field.

1. Introduction

In recent years, the interest of researchers has been focused on studying caloric effects (CE) in solid state materials [1–7]. The demonstration of CEs is expressed in changing temperature and/or entropy under external magnetic, electric or elastic fields [8,9]. The materials with at least two CEs are called multicaloric ones [10]. Multiferroics combining spin-charge ordered structures are possible materials for realization of CE. The most well-known multiferroics are BiFeO_3 -based (BFO) compositions obtained in course of partial isovalent substitution of bismuth for rare-earth ions [11]. In this case, the increase in the resultant magnetic moment and the enhancement of

magnetolectric interaction are observed. A lot of structural varieties, depending on the method and conditions of preparation, as well as concentration-related changes in physical properties were found in the $\text{Eu}_x\text{Bi}_{1-x}\text{FeO}_3$ (EuBFO) system [12,13]. The choice of Eu^{3+} as a doping ion is due to a small ionic radius relative to the radius of the replaced Bi^{3+} ion [14]. This leads to the appearance of large structural distortions in BFO, which increases the intensity of magnetic interactions according to the crystal and chemical approach due to a change in the lengths of interionic bonds and values of Fe–O–Fe bond angles [15,16]. This fact, as well as the high magnetoactivity of Eu^{3+} ion lead to the formation of ferromagnetically ordered state in EuBFO even with a low degree of cation substitution. According to the availability of

* Corresponding authors at: State Key Laboratory of Superhard Materials, International Centre of Future Science of Jilin University, 130012 Changchun, China (N.A. Liedienov).

E-mail addresses: igmak2010@yandex.by (I.I. Makoed), nikita.ledenev.ssp@gmail.com (N.A. Liedienov).

<https://doi.org/10.1016/j.jmmm.2019.165379>

Received 23 April 2019; Received in revised form 18 May 2019; Accepted 29 May 2019

Available online 30 May 2019

0304-8853/ © 2019 Elsevier B.V. All rights reserved.

noticeably features in the temperature dependences of the magnetization [17] and heat capacity at Neel temperature [18], EuBFO samples are of interest and can be considered as thermo-magnetic materials.

It should be also noted that at small $x < 0.10$ degrees of substitution of Bi^{3+} for Eu^{3+} cations, EuBFO samples crystallize in a rhombohedral R3c lattice which is an isostructural one for BFO lattice [19–21]. At $x > 0.10$, concentration transitions in *Pnma* [19], *Pn21a* [20], *P1* [21] structures are observed in EuBFO. Analysis of these data shows that samples of the same composition, but synthesized under different conditions have different structural and physical properties. It is due to the high sensitivity of structural factors to small changes of the composition. Therefore, the investigation of the isostructural EuBFO samples synthesized at the same temperature, time and pressure is of particular interest.

The aim of this work is an experimental and theoretical investigations on the evolution of structure, magnetic phase transitions, magnetic properties and magnetocaloric (MC) effect in the $\text{Eu}_x\text{Bi}_{1-x}\text{FeO}_3$ ($x = 0\text{--}0.20$) samples depending on the degree of substitution, temperature, and magnetic field.

2. Experimental section

The polycrystalline EuBFO samples with a concentration of $x = 0.00$ (BFO), 0.05 (EuBFO5), 0.10 (EuBFO10), 0.15 (EuBFO10) and 0.20 (EuBFO10) were synthesized using the solid-state reaction route [22]. The initial Eu_2O_3 , Bi_2O_3 and Fe_2O_3 powders (chemical purity 99.99%, Sigma Aldrich Chemicals) were mixed for 0.5 h in a stoichiometric ratio in a dried agate mortar and after wards for 2 h with ethanol. The obtained mixture was preliminary synthesized at a temperature of $850 \pm 50^\circ\text{C}$ in a ceramic vessel in air for 5 h. The heating rate was $10^\circ\text{C}/\text{min}$. After grinding and repeated synthesizing under the same conditions, X-ray diffraction studies of the obtained mixture for controlling the phase composition were carried out. After that the samples were finally annealed from preliminary synthesized and grinded mixture under cold pressing at high pressure $P = 4$ GPa for 1 min using a high-pressure equipment (see Supplementary material, Figs. 1S and 2S).

Studies of microstructure and chemical composition were performed from the external (outside) and internal (breaking of the pellets and placing them vertically to see internal structure) surfaces of the samples using Hitachi S-3000N and FEI Magellan 400 scanning electron microscope (SEM) with energy dispersive X-ray spectroscopy module. The type and parameters of crystal lattice were determined on the basis of a full-profile analysis of diffraction patterns obtained by DRON-3M diffractometer in $\text{CuK}\alpha$ radiation at room temperature. The analysis and refinement of X-ray data were performed by JANA2006 software using Rietveld method [23].

Magnetic-field dependences of a specific magnetization were studied by SQUID magnetometer (Superconducting Quantum Interference Device, LOT-Quantum Design MPMS-XL) and a vibration magnetometer (VSM, OXFORD) at temperatures of 5 K, 100 K and 300 K in magnetic fields up to $H = 4$ T. The temperature dependences of the magnetization for the samples placed in vacuum quartz ampoules were measured by Faraday method [24] within the temperature range of $T = 300\text{--}1000$ K in a magnetic field of $H = 0.86$ T.

3. Results and discussion

3.1. Structural properties

The results of a full-profile analysis of X-ray patterns are shown in Fig. 1(a–e). At $x < 0.10$, the replacement of bismuth by europium cations leads to the stabilization of crystal lattice and the obtaining samples with a predominant content of the R3c phase. The presence of $\text{Bi}_2\text{Fe}_4\text{O}_9$ impurity was observed in a pure BFO, which does not exhibit ferromagnetic/ferrimagnetic and ferroelectric properties at

temperatures higher than 250 K [25,26]. The traces of the initial Bi_2O_3 , Fe_2O_3 and Eu_2O_3 oxides were not detected, which indicates their complete polymorphic transformation. The obtained values of the lattice parameters (see Table 1) correspond well with the known data [20].

As can be seen from Table 1, the structural factors are sensitive to small changes of the composition. The calculated values of the lattice parameters for the BFO–EuBFO10 samples are systematically reduced, which is caused by 4*f*-compression effect [27] due to a change in the average value of the effective radii of cations at the isovalent replacement of bismuth by europium cations. The diffraction maxima shift to the region of high angles with increasing x . The reason for the significant effect of the composition on morphological changes is the difference in the radii of the Bi^{3+} ($r = 1.17 \text{ \AA}$) and Eu^{3+} ($r = 1.07 \text{ \AA}$) cations [14], which was also observed in [11,13,20]. The same behavior is demonstrated for the EuBFO15 and EuBFO20 samples which crystallize in a *Pn21a* structure.

The EuBFO5 and EuBFO10 samples are single-phased and crystallize in a non-centrosymmetric rhombohedral crystal lattice with R3c space group (JCPDS no: 71-2494). In the X-ray patterns for the EuBFO15 and EuBFO20 samples, a shift of peaks, an appearance of new maximum at $2\theta \approx 25^\circ$ and a split of maximum at $2\theta = 32^\circ$ are observed. The results of a full-profile analysis of X-ray patterns confirm the fact of crystallization of the EuBFO15 and EuBFO20 samples in the orthorhombic *Pn21a* crystal structure and the presence of a concentration phase transition from R3c to *Pn21a*. The space group *Pn21a*, as well as R3c is non-centrosymmetric, and it may have a polar ion displacement along the axis (0 1 0) leading to a charge ordered state. For all compositions with increase in the Eu concentration, a reduction of a unit cell volume associated with a change in the Fe–O bond lengths and the Fe–O–Fe bond angles is observed.

According to SEM data obtained outside and inside of the EuBFO ceramics, there is no clearly defined microstructure for the external surface (see Fig. 2(a), (c), (e), (g)) in contrast to the images obtained for the internal surface (see Fig. 2(b), (d), (f), (h)). It may be related to the preparation method of the EuBFO samples synthesized under high $P = 4$ GPa. With increase in the Eu concentration a decrease in the grain size is observed, which is possibly due to the difference between bond dissociation energy of Bi–O (343 ± 6 kJ/mol) and Eu–O (557 ± 12 kJ/mol) [13].

According to EDS data (see Fig. 3) the chemical composition of the EuBFO agrees approximately with nominal composition 1:1:3. The measured atomic percentages of Eu, Bi, Fe and O are 0.52%, 17.68%, 16.98% and 64.81% for EuBFO5; 1.91%, 16.75%, 17.21% and 64.13% for EuBFO10; 2.42%, 14.66%, 14.80% and 68.12% for EuBFO15 as well as 3.34%, 15.89%, 16.86% and 63.91% for EuBFO20, respectively.

3.2. Magnetic properties and magnetocaloric effect

Appearance of a weak ferromagnetic (wFM) moment in the EuBFO is caused by, firstly, the suppression of spin cycloid due to partial substitution of bismuth for europium cations in the BFO and, secondly, the violation of collinearity (angularity) of antiferromagnetically (AFM) ordered magnetic moments in Fe^{3+} (*d*-subsystem) and Eu^{3+} (*f*-subsystem) sublattices. Therefore, the contribution from the spin subsystems to the total energy of crystal is [28]:

$$\Delta E = \sum_{i \neq j} J_{ij} (\mathbf{S}_i \cdot \mathbf{S}_j) + \sum_{i \neq j} \mathbf{D}_{ij} [\mathbf{S}_i \cdot \mathbf{S}_j] - \mu_B g_L \sum_i (\mathbf{H} \cdot \mathbf{S}_i), \quad (1)$$

where \mathbf{S}_i , \mathbf{S}_j are magnetic moments of Fe^{3+} and Eu^{3+} cations, respectively; J_{ij} is an exchange integral; \mathbf{D}_{ij} is Dzyaloshinskii-Moriya vector [29,30]; μ_B is Bohr magneton; g_L is Lande factor; \mathbf{H} is an external magnetic field. The first term in an Eq. (1) is due to asymmetric exchange interaction which determines AFM ordering in *d*- and *f*-subsystems at temperatures below Néel point (T_N). AFM ordering spin magnetic moments of Eu cations is observed at temperatures below

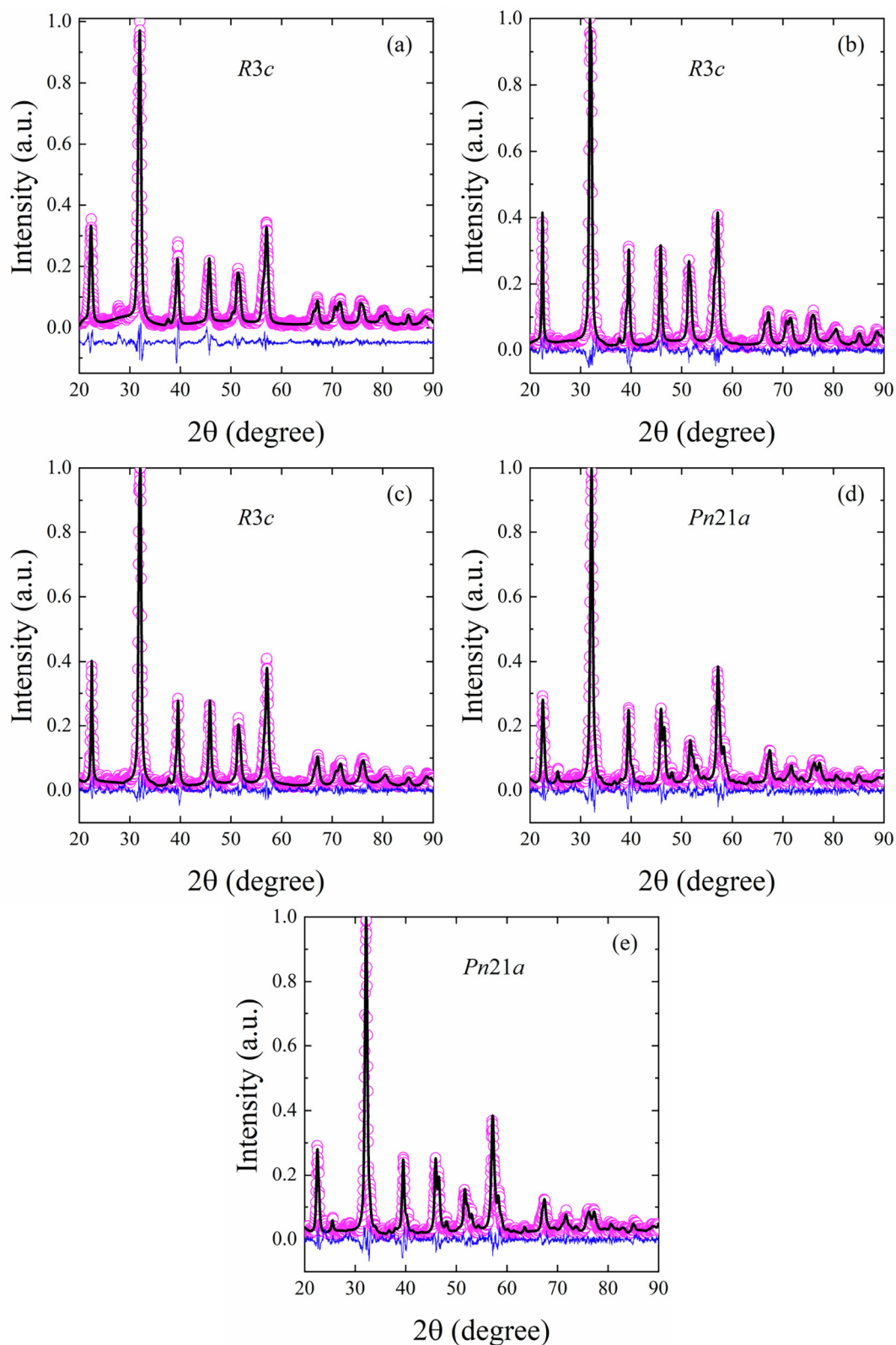


Fig. 1. X-ray patterns of the BFO (a), EuBFO5 (b), EuBFO10 (c), EuBFO15 (d) and EuBFO20 (e) samples obtained at room temperature.

10 K [31] that is much lower than the ordering temperature of d -subsystems in the EuBFO because $\text{Eu}^{3+}-\text{O}^{2-}-\text{Eu}^{3+}$ exchange interaction is weaker than $\text{Fe}^{3+}-\text{O}^{2-}-\text{Fe}^{3+}$ [32]. The second term in the Eq. (1) describes Dzyaloshinskii-Moriya interaction, contribution of which to ΔE equals to a few percent from exchange interaction energy [28]. This contribution determines the magnitude of slope of AFM ordered

magnetic moments and, as a consequence, the resultant wFM moment value. The third term in the Eq. (1) describes the interaction between \mathbf{S}_i magnetic moments and \mathbf{H} external magnetic field.

Within the framework of the phenomenological model proposed by Hamad [33], the temperature dependence of magnetization (M) in the vicinity of Néel point can be written as:

Table 1

The lattice parameters (Å), unit cell volume (Å³), and X-ray density (g/cm³) for the EuBFO samples obtained by the Rietveld refinement of X-ray patterns.

Composition	Space group	Structural parameters and criteria of fit							
		a (Å)	b (Å)	c (Å)	V (Å ³)	ρ (g/cm ³)	GOF	R _p (%)	R _{wp} (%)
BFO	R3c	5.6200	5.6200	13.6920	374.5	8.3247	1.15	17.09	23.01
EuBFO5	R3c	5.5803	5.5803	13.8220	372.7	8.2886	1.20	13.78	18.65
EuBFO10	R3c	5.5758	5.5758	13.7828	371.1	8.2478	1.20	13.30	17.97
EuBFO15	Pn21a	5.5945	7.9095	5.4463	241.0	8.3882	1.20	14.33	19.05
EuBFO20	Pn21a	5.6072	7.8822	5.4258	239.8	8.3512	1.32	15.61	20.14

$$M = \left(\frac{M_i - M_f}{2} \right) \tanh[A(T_N - T)] + BT + C, \quad (2)$$

where M_i and M_f are initial and final points of temperature range of wFM-AFM transition. The values of A , B , C are defined as $A = \frac{2(B - S_N)}{M_i - M_f}$,

$$B = \left(\frac{dM}{dT} \right)_T \text{ and } C = \left(\frac{M_i + M_f}{2} \right) - BT_N, \text{ where } S_N = \left(\frac{dM}{dT} \right)_{T_N}.$$

The magnetic contribution to magnetic entropy change (ΔS_M) depends on the value of an external magnetic field from 0 to H_{\max} :

$$\Delta S_M = \left\{ -A \left(\frac{M_i - M_f}{2} \right) \operatorname{sech}^2[A(T_N - T)] + B \right\} H_{\max}. \quad (3)$$

The maximum value of ΔS_M contribution is reached at temperature $T = T_N$ and defined as:

$$\Delta S_{\max} = \left\{ -A \left(\frac{M_i - M_f}{2} \right) + B \right\} H_{\max}, \quad (4)$$

and a full-width at half-maximum of the peak (δT_{FWHM}) is determined from the following expression:

$$\delta T_{\text{FWHM}} = \frac{2}{A} \operatorname{sech} \left[\sqrt{\frac{2A(M_i - M_f)}{A(M_i - M_f) + 2B}} \right]. \quad (5)$$

The magnetic cooling efficiency based on the magnetic entropy change is assessed from the values of relative cooling power (RCP):

$$RCP = -\Delta S_M(T, H_{\max}) \cdot \delta T_{\text{FWHM}}. \quad (6)$$

The change in a magnetic part of specific heat capacity ($\Delta C_{p,H}$) is calculated as:

$$\Delta C_{p,H} = -2TA^2 \left(\frac{M_i - M_f}{2} \right) \operatorname{sech}^2(A(T_N - T)) \tanh(A(T_A - T)) H_{\max}. \quad (7)$$

Above the magnetic ordering T_N point, the contribution to the resultant magnetization due to the corresponding spin reorientation process is eliminated. The behavior of $M(T)$ curve (see Fig. 4) obtained as the result of simulation in every range of $T < T_N$, $T_N < T_{N1}$ and $T_{N1} < T$ can be interpreted as the resultant magnetization which is due to fluctuations in the directions of spin moments of magnetically active cations within the corresponding magnetic transition regions. Consequently, the thermodynamic characteristics, assessed from the Eqs. (2)–(7) and calculated at T_{N1} and T_{N2} points, include contributions from the rearrangement of spin structure for two magnetic phase transitions which are “weak ferromagnetic-antiferromagnetic” (wFM-AFM) and “antiferromagnetic-paramagnetic” (AFM-PM) within the temperature ranges 640–650 K and 818–822 K, respectively. The model parameters for describing the behavior of a specific magnetization within the wFM-AFM transition region are listed in Table 2.

The results of the $M(T)$ curve simulated within the AFM-PM transition confirm the independence of the model parameters from the concentration of Eu cations. The average value of T_{N2} transition temperature is 820 ± 2 K. While using the average values of $B = (-3.15 \pm 0.13) \cdot 10^{-5}$ emu/g·K and $S_N = (-1.20 \pm 0.05) \cdot 10^{-4}$ emu/g·K, MC characteristics of $-\Delta S_M = (1.03 \pm 0.05) \cdot 10^{-4}$ J/kg·K, $RCP = (3.20 \pm 0.09) \cdot 10^{-4}$ J/kg and $\Delta C_{p,H} = (4.80 \pm 0.09) \cdot 10^{-3}$ J/

kg·K were calculated. The availability of magnetic phase transition in similar materials at temperature 890 K was also described in [34]. The shape of $M(H)$ field dependences [34] does not confirm the presence of ferromagnetic order (open loops of ferromagnetic hysteresis are absent) within this temperature range, which also gives grounds to relate this anomaly $M(T)$ to the AFM-PM transition. The displacement of the transition point $T_{N2} \approx 820$ K is due to the different method of preparation. The similar results confirming the presence of a magnetic transformation in BFO samples with Nd at a temperature of 820 K are also given in [35].

The temperature dependences of the MC characteristics within the wFM-AFM transition range are shown in Figs. 5–7.

The curves are typical in shape for all compositions, but have certain differences depending on the concentration of replacement cations. With increase in the degree of substitution, there is a redistribution of the intensities of the maximum values of ΔS_M , RCP , $\Delta C_{p,H}$ and their shift in the temperature according to the values of T_{N1} . The concentration dependences of the change in the full-width at half-maximum of the peak δT_{FWHM} and the temperature change of ΔT_{\max} at T_{N1} are presented in Fig. 8. In order to estimate the value of temperature change (see Fig. 8) at the MC effect, the formula $\Delta T_{\max} = -(T/C_{p,H}) \cdot \Delta S_M$ was used. The value $C_{p,H}$ is 0.4 J/kg·K for BFO ceramic sample. The maximum values of the absolute values for ΔS_M and $\Delta C_{p,H}$ are observed in the EuBFO15 composition, i.e. near the structural transition at the conditions of coexistence of R3c and Pn21a phases. The minimum values of the ΔS_M and $\Delta C_{p,H}$ contributions, which are even lower than in the BFO, are obtained in the EuBFO5 and EuBFO10 compositions. Relatively low RCP values are observed in the BFO and EuBFO5 samples with narrow temperature intervals of the wFM-AFM transition, which are characterized by low δT_{FWHM} values relative to the maximum value for the EuBFO20. The largest RCP is observed in the EuBFO20 sample.

The results of the calculation indicate that absolute values of ΔS_M , RCP , $\Delta C_{p,H}$ are relatively small in the vicinity of the T_{N1} point. The values of RCP and $\Delta C_{p,H}$ are fractions of a percent, and the values of ΔS_M are units of a percent from the values of the respective contributions formed at the wFM-AFM transition in a magnetic field $H = 0.86$ T.

For a more in-depth analysis of the obtained MC data, the magnetic field dependences of the specific magnetizations for the EuBFO samples were additionally investigated (see Figs. 9 and 10). A residual magnetization (M_r) gradually increases with increasing Eu concentration in the BFO system, which confirms the presence of wFM.

The shape of the hysteresis loops of the specific magnetization for the EuBFO samples indicates the presence of various types of magnetoactive interactions, i.e. wFM and AFM in the magnetic sublattice formed by Fe^{3+} cations and PM due to the interaction of Eu^{3+} cations in the rare-earth sublattice. In order to separate the wFM and AFM/PM contributions, the hysteresis loops were simulated using equation [36]:

$$M(H) = \frac{2M_s}{\pi} \tan^{-1} \left[\frac{H \pm H_C}{H_C} \tan \left(\frac{\pi S}{2} \right) \right] + \chi H. \quad (8)$$

The first term in the Eq. (8) describes the wFM component, and the second one determines the linear contributions from the AFM and PM interactions. The parameter S characterizes the rectangularity of the magnetization loop defined as the ratio of the residual magnetization

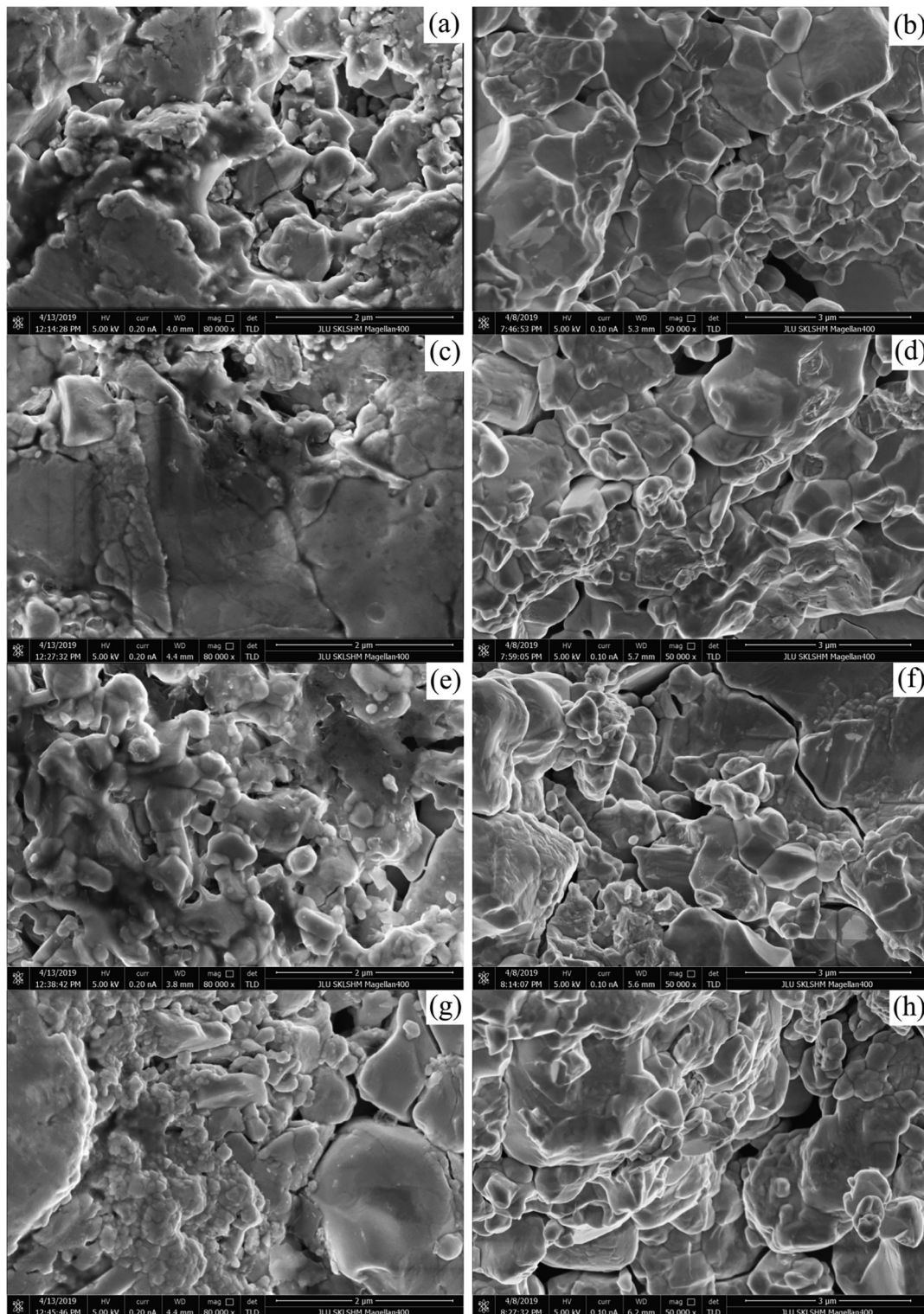


Fig. 2. SEM images obtained outside and inside of the EuBFO ceramics for EuBFO5 (a) and (b), EuBFO10 (c) and (d), EuBFO15 (e) and (f), EuBFO20 (g) and (h), respectively.

M_r to the saturation magnetization M_s ; H_C is a coercive force; χ is a magnetic susceptibility. It should be noted that the saturation of the magnetization is not achieved on the experimental dependencies up to 4 T. Therefore, the parameters of M_s at the simulation were varied with a purpose to get the best result. The values of M_r and H_C were obtained from the partial hysteresis loops. The inset of Fig. 10 shows the simulated results for a hysteresis loop to separate the wFM and AFM/PM contributions for the EuBFO20 sample. The model parameters are

shown in Table 3.

The enhancement of the magnetic properties in course of ion replacement is due to a combination of several factors. Firstly, a structural phase transformation of $R3c-Pn21a$ causes the slope of the FeO_6 octahedra and, as a result, leads to a change in the values of the Fe–O–Fe angles. The magnitude of the Fe–O–Fe bond angle determines the conditions of the magnetic exchange interaction that occurs through the orbital overlap between Fe^{3+} and O^{2-} ions. This leads to an increase in

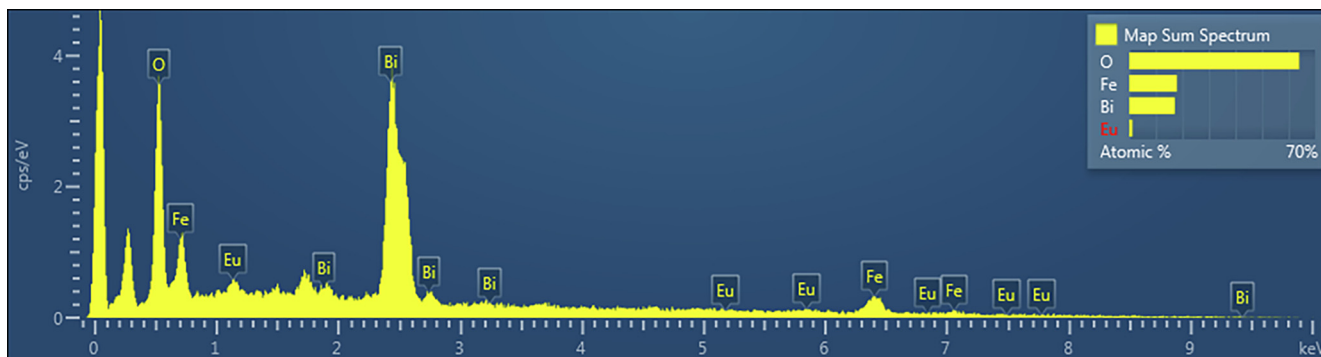


Fig. 3. Typical EDS pattern for the EuBFO ceramics at the example of the EuBFO10.

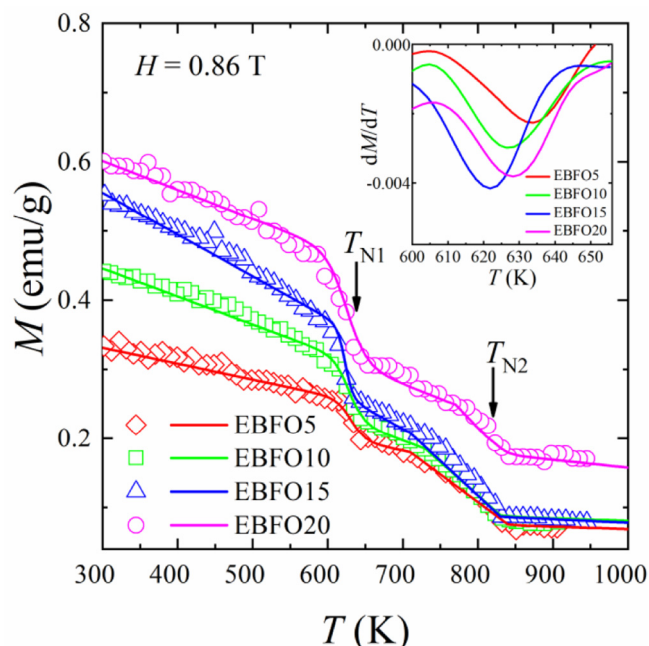


Fig. 4. Temperature dependences of specific magnetization, $M(T)$, for the EuBFO samples. The simulated curves obtained from the Eq. (2) are indicated by a solid line. The inset shows temperature dependences dM/dT for determining T_{N1} .

Table 2

The model parameters for describing temperature dependences of specific magnetization within the wFM-AFM transition range.

Composition	M_i (emu/g)	M_f (emu/g)	$B \cdot 10^{-5}$ (emu/g·K)	S_N (emu/g·K)	T_{N1} (K)
BFO	0.099	0.073	-1.2	-0.0024	631
EuBFO5	0.255	0.198	-23.0	-0.0017	631
EuBFO10	0.313	0.226	-50.0	-0.0022	628
EuBFO15	0.360	0.260	-60.4	-0.0053	623
EuBFO20	0.465	0.310	-42.0	-0.0033	625

the slope angle of adjacent AFM ordered planes and the wFM interactions. Secondly, the change in the mutual arrangement of the spin magnetic moments of the Fe^{3+} cations is associated with a change in the conditions of the antisymmetric exchange interaction of the Dzyaloshinskii-Moriya. In an ideal cubic perovskite, this contribution is equal to zero due to the equality of the 180° bond angle $Fe-O-Fe$ [37]. As the magnitude of this angle changes, the magnitude of the magnetization increases because of the phase transition from the AFM to the wFM state. The third factor is the PM contribution of the large magnetic moment in the saturation state of Eu^{3+} ($7\mu_B$) ions to magnetization.

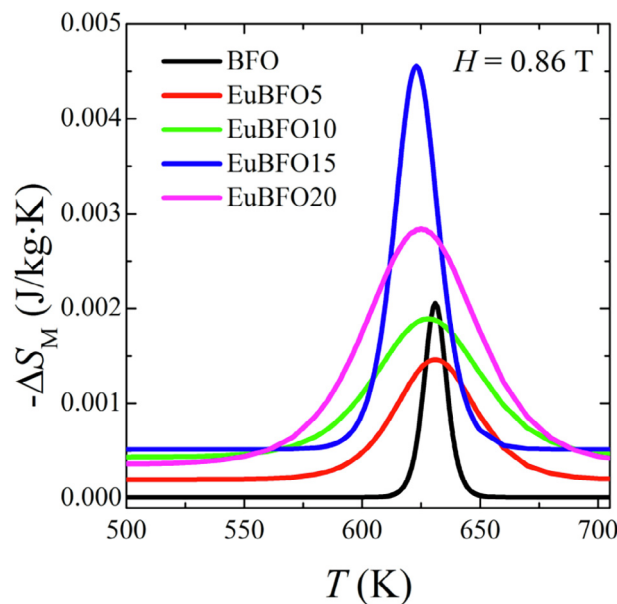


Fig. 5. Temperature dependences of magnetic entropy change, $\Delta S_M(T)$, for the EuBFO samples.

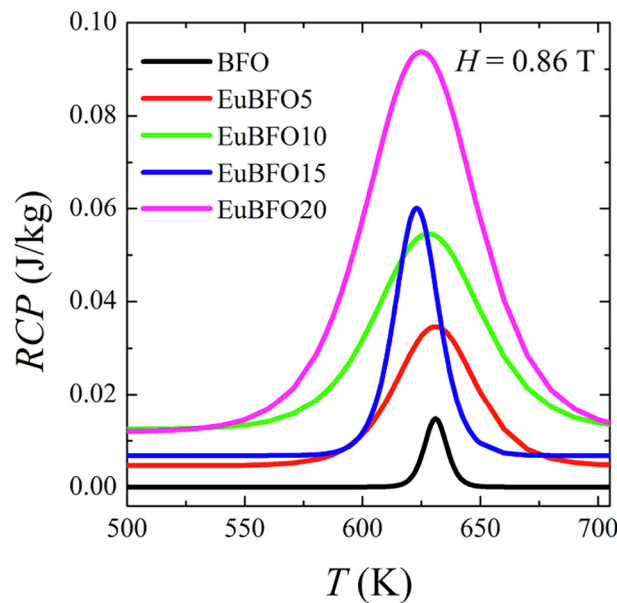


Fig. 6. Temperature dependences of the relative cooling power, $RCP(T)$, for the EuBFO samples.

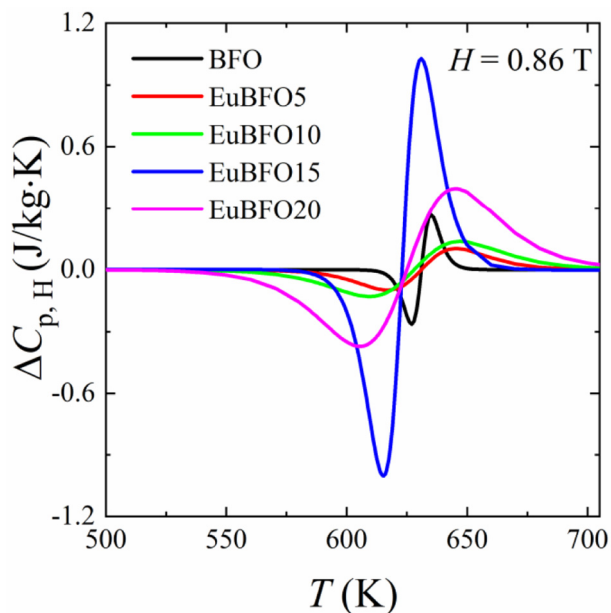


Fig. 7. Temperature dependences of specific heat capacity change, $\Delta C_{p,H}(T)$, for the EuBFO samples.

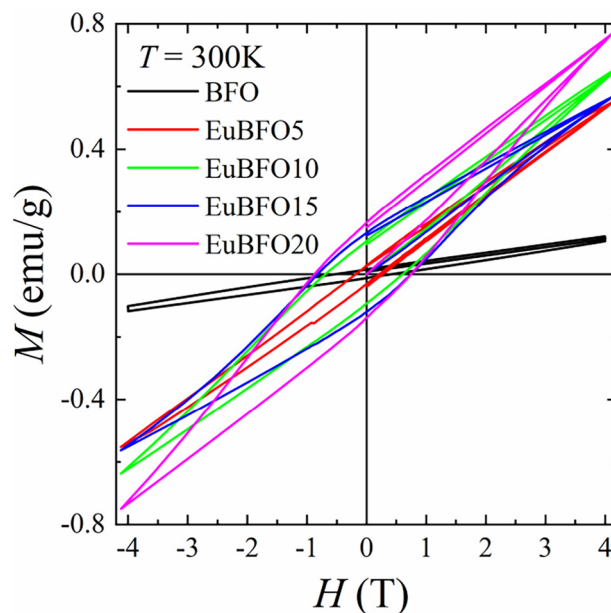


Fig. 9. Magnetic field dependences of the specific magnetization, $M(H)$, for the EuBFO samples at temperature of 300 K.

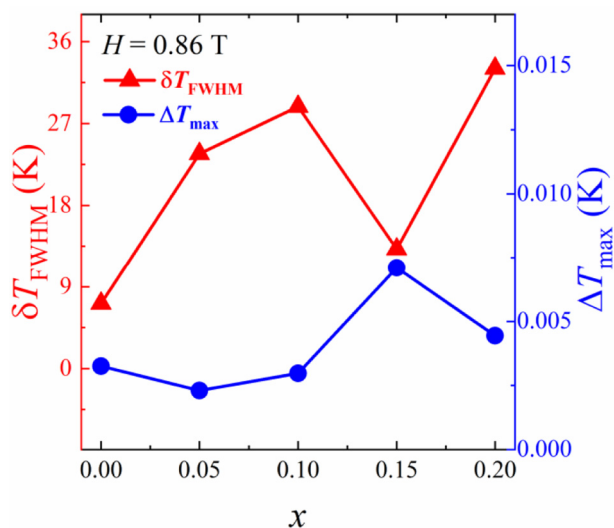


Fig. 8. Concentration dependencies of the full-width at half-maximum, $\delta T_{FWHM}(x)$, and the maximum temperature change, $\Delta T_{max}(x)$, for the EuBFO within wFM-AFM transition range.

The AFM order in the system can be described as a result of the coexistence of two spin sublattices with FM interaction in each sublattice and AFM interaction between the sublattices. The model of two sublattices leads to a long-range collinear antiparallel spin structure with a zero magnetic moment due to the complete compensation of the spin moments of these sublattices. Incomplete spin compensation of these sublattices can occur in the AFM BFO when bismuth cations are replaced. Substitution of Bi^{3+} cations leads to suppression of the spatial spin-modulated structure and the appearance of the wFM response in the EuBFO compositions, the value of which depends on the concentration of Eu^{3+} cations. As follows from the magnetic data analysis, the contribution of the wFM ordering increases with increasing content of Eu^{3+} cations and achieves the maximum in the EuBFO20 sample. The evolution of the contributions of the AFM/PM components to the resultant magnetization is illustrated in Figs. 11 and 12 plotted on the basis of the calculated data according to the Eq. (8).

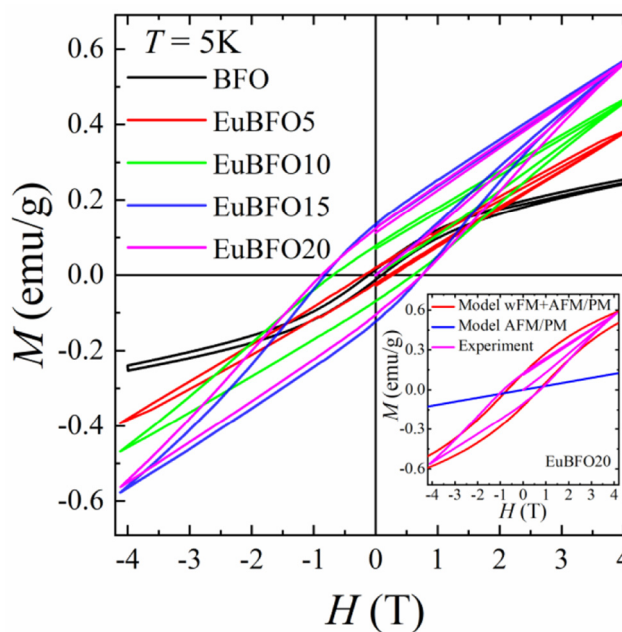


Fig. 10. Magnetic field dependences of the specific magnetization, $M(H)$, for the EuBFO samples at temperature of 5 K. The inset indicates the simulation results for a hysteresis loop to separate the wFM and AFM/PM contributions for the EuBFO20 sample.

At a temperature of 5 K, the AFM/PM contribution increases with increasing concentration of Eu^{3+} for the EuBFO15, and then decreases for the EuBFO20 sample. The decrease in the magnitude of this contribution to the magnetization of EuBFO20 is due to increasing the fraction of the $Pn21a$ phase. This phase provides the establishment of the collinear AFM ordering, when the spiral ordering of the spin magnetic moments of d -sublattice is destroyed. There is a linear increase in the value of the AFM/PM contribution at room temperature, which reaches the highest value in EuBFO20. The concentration dependences of the magnetic characteristics for the samples are presented in Figs. 13 and 14.

Significant differences in the dependences of $\mu_0 H_C(T)$ obtained at

Table 3
The model parameters for describing the magnetic field dependences of the specific magnetization.

Composition	T = 5 K				T = 300 K			
	M_s (emu/g)	$\mu_0 H_C$ (T)	M_r (emu/g)	$\chi, 10^{-6}$ (emu/g·K)	M_s (emu/g)	$\mu_0 H_C$ (T)	M_r (emu/g)	$\chi, 10^{-6}$ (emu/g·K)
BFO	0.300	0.127	0.014	0.700	0.350	0.589	0.015	0.700
EuBFO5	0.610	0.209	0.019	2.000	0.650	0.200	0.028	3.370
EuBFO10	0.810	0.711	0.076	2.600	0.820	0.678	0.107	4.200
EuBFO15	0.750	0.831	0.135	3.000	0.640	0.806	0.132	3.200
EuBFO20	0.710	0.836	0.122	2.400	0.940	0.886	0.166	4.830

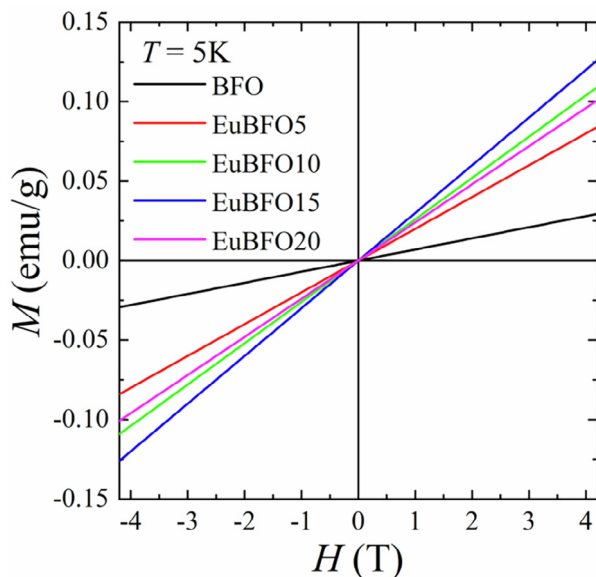


Fig. 11. Magnetic field dependences of AFM/PM contributions to the specific magnetization, $M(H)$, for the EuBFO samples at a temperature of 5 K.

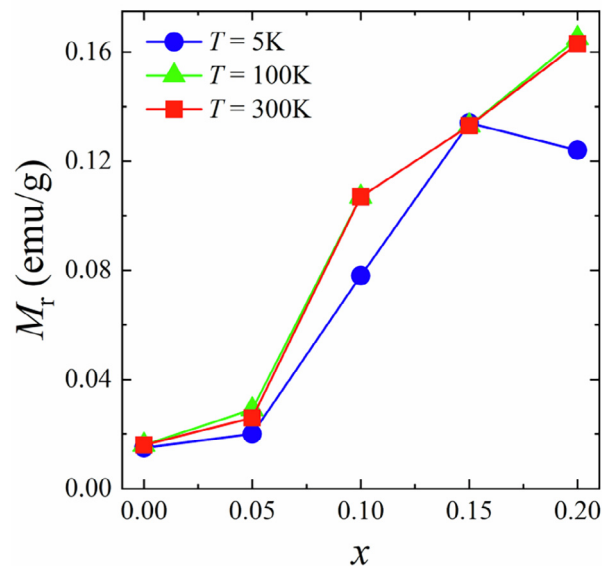


Fig. 13. Concentration dependences of the residual specific magnetization, $M_r(x)$, for the EuBFO samples.

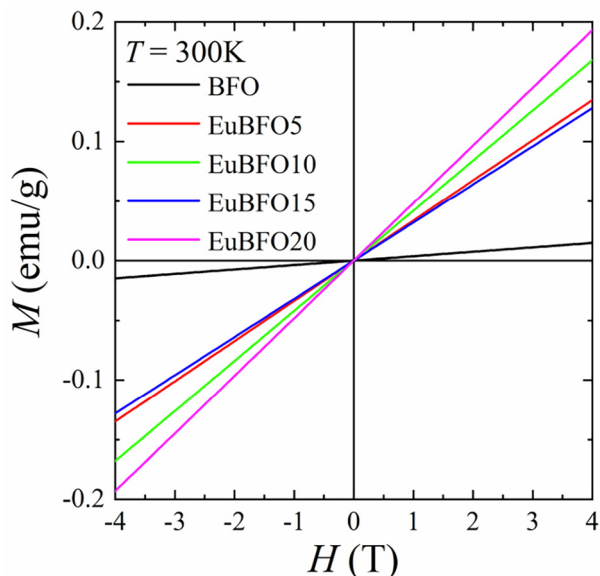


Fig. 12. Magnetic field dependence of AFM/PM contributions to the specific magnetization, $M(H)$, for the EuBFO samples at a temperature of 300 K.

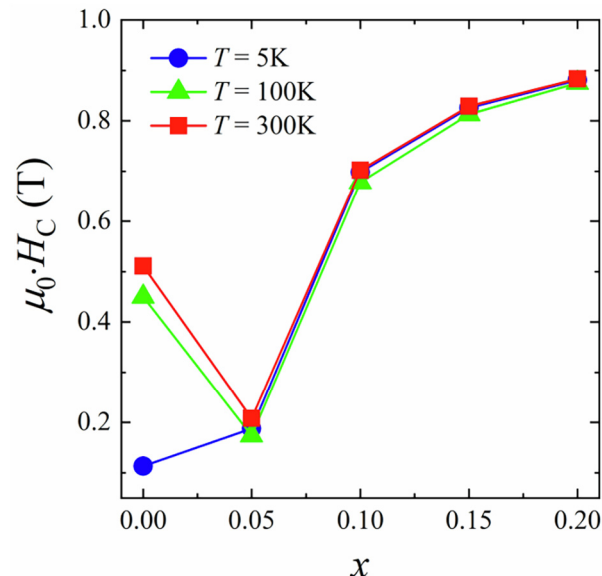


Fig. 14. Concentration dependences of coercive field, $H_c(x)$, for the EuBFO samples.

5 K are explained by the effect of the disordered spin moments of europium cations at temperatures higher than 10 K [31]. An isovalent substitution of Bi^{3+} with Eu^{3+} cations in the BFO leads to the suppression of the spatial spin-modulated structure and the appearance of

the wFM response. The change in the behavior of the $M_r(x)$ is associated with the structural transition, in which the AFM/PM and the wFM ordered states coexist. The composition of the cation sublattices affects significantly the intersublattice $\text{Eu}(\text{Bi})\text{-O-Eu}(\text{Bi})$ and intrasublattice Fe-O-Fe exchange interactions. A change in the bond lengths of Eu-O

and Fe–O and, as a result, the magnitudes of the Fe–O–Fe angles causes a change in the conditions of indirect, through the oxygen, AFM exchange interactions. The distortions of the initial BFO matrix due to the size factor induce a noticeable increase in the values of the specific residual magnetization and the coercive force of the individual magnetic hysteresis loops.

4. Conclusions

X-ray diffraction, SEM and magnetic methods have been used for investigating the structure, microstructure, magnetic properties and magnetocaloric effect in the ceramic $\text{Eu}_x\text{Bi}_{1-x}\text{FeO}_3$ samples with a concentration of $x = 0\text{--}0.2$ prepared by a solid-state reaction method under cold pressing at high pressure $P = 4$ GPa.

It has been shown that with increase in the concentration x of Eu ions the crystal structure of the $\text{Eu}_x\text{Bi}_{1-x}\text{FeO}_3$ compositions is distorted and at $x = 0.15$ a structural phase transition from a rhombohedral $R3c$ to an orthorhombic $Pn21a$ perovskite structure is observed. Microstructure and chemical composition of the $\text{Eu}_x\text{Bi}_{1-x}\text{FeO}_3$ samples have been clarified by SEM data.

According to magnetic data, the temperature dependences of magnetization for the $\text{Eu}_x\text{Bi}_{1-x}\text{FeO}_3$ multiferroics show two magnetic “weak ferromagnetic-antiferromagnetic” at $T_{N1} = 640\text{--}650$ K and “antiferromagnetic-paramagnetic” at $T_{N2} = 818\text{--}822$ K phase transitions. The appearance of a weak ferromagnetism is caused by suppression of the spatial spin-modulated structure in course of an isovalent substitution of Bi^{3+} with Eu^{3+} cations in the $\text{Eu}_x\text{Bi}_{1-x}\text{FeO}_3$. Magnetic entropy change, heat capacity change, relative cooling power and full-width at half-maximum of the peak have been determined. It has been established that the thermodynamic characteristics are relatively small in the vicinity of the T_{N1} point and strongly depend on the concentration, temperature and magnetic field. The EuBFO15 and EuBFO20 compositions have maximum values of magnetocaloric characteristics because of structural phase transition from $R3c$ to $Pn21a$.

The results of the investigations of the magnetic properties for the $\text{Eu}_x\text{Bi}_{1-x}\text{FeO}_3$ samples confirm the presence of the magnetocaloric effect and indicate the possibility of its practical application at temperatures above room temperature. The obtained data can be used to study the magnetocaloric effect and the features of phase magnetic transitions in similar materials.

Acknowledgments

This work was performed within the framework of State Scientific Research Program 2016–2020 “Physical materials science, new materials and technology” (“Material Science and technology of materials” subprogram, task No. 1.35), Belarus, and supported by Russian Science Foundation (project № 18-79-10176) for support theoretical studies of magnetic and magnetocaloric properties, Russia, and Chinese Program “The Thousand Talents Program for Foreign Experts” Project WQ20162200339, China. The authors also gratefully acknowledge the financial support of the Ministry of Education and Science of the Russian Federation in the framework of Increase Competitiveness Program of NUST «MISI» (NoK4-2018-036, P02-2017-2-4), implemented by a governmental degree dated 16th of March 2013, No 211, Russia.

Appendix A. Supplementary data

Supplementary data to this article can be found online at <https://doi.org/10.1016/j.jmmm.2019.165379>.

References

[1] X. Moya, L.E. Hueso, F. Maccherozzi, A.I. Tovstolytkin, D.I. Podyalovskii, C. Ducati, L.C. Phillips, M. Ghidini, O. Hovorka, A. Berger, M.E. Vickers, E. Defay, S.S. Dhesi,

N.D. Mathur, Giant and reversible extrinsic magnetocaloric effects in $\text{La}_{0.7}\text{Ca}_{0.3}\text{MnO}_3$ films due to strain, *Nat. Mater.* 12 (2013) 52–58.

[2] G. Suchanek, V. Pakhomov, G. Gerlach, *Electrocaloric Cooling*, Chapter 2 in Book: Refrigeration, Orhan Ekren, Intech. Open, 2017.

[3] A. Chauhan, S. Patel, R. Vaish, C.R. Bowen, A review and analysis of the elastocaloric effect for solid-state refrigeration devices: challenges and opportunities, *Mater. Res. Soc.* 2 (2015) 1–18.

[4] A.M. Tishin, Y.I. Spichkin, *The Magnetocaloric Effect and its Applications*, Institute of Physics Publishing, Bristol and Philadelphia, 2003, p. 476.

[5] A.V. Pashchenko, N.A. Liedienov, Quanjun Li, D.D. Tatarchuk, V.A. Turchenko, I.I. Makoed, V.Ya. Sycheva, A.V. Voznyak, V.P. Kladko, A.I. Gudimenko, Y.V. Didenko, A.T. Kozakov, G.G. Levchenko, Structure non-stoichiometry, valence of ions, dielectric and magnetic properties of single-phase $\text{Bi}_{0.9}\text{La}_{0.1}\text{FeO}_{3-\delta}$ multiferroics, *J. Magn. Magn. Mater.* 483 (2019) 100–113.

[6] E.L. Fertman, A.V. Fedorchenko, D.D. Khalyavin, A.N. Salak, A. Baran, V.A. Desnenko, O.V. Kotlyar, E. Čizmár, A. Feher, E.S. Syrkin, A.I. Vaisburd, N.M. Olekhovich, A.V. Pushkarev, Yu.V. Radyush, A. Stanulis, A. Kareiva, Multiferroic $\text{Bi}_{0.65}\text{La}_{0.35}\text{Fe}_{0.5}\text{Sc}_{0.5}\text{O}_3$ perovskite: magnetic and thermodynamic properties, *J. Magn. Magn. Mater.* 429 (2017) 177–181.

[7] V. Markovich, A. Wisniewski, H. Szymczak, Chapter one – magnetic properties of perovskite manganites and their modifications, *Handb. Magn. Mater.* 22 (2014) 1–201.

[8] X. Moya, S. Kar-Narayan, N.D. Mathur, Caloric materials near ferroic phase transitions, *Nat. Mater.* 13 (2014) 439–450.

[9] V. Franco, J.S. Blázquez, J.J. Ipus, J.Y. Law, L.M. Moreno-Ramírez, A. Conde, Magnetocaloric effect: from materials research to refrigeration devices, *Prog. Mater. Sci.* 93 (2018) 112–232.

[10] M.M. Vopson, The multicaloric effect in multiferroic materials, *Solid State Commun.* 152 (2012) 2067–2070.

[11] D.C. Arnold, Composition-driven structural phase transitions in rare-earth-doped BiFeO_3 ceramics: a review, *IEEE Trans. Ultrason. Ferroelectr. Freq. Control* 62 (2015) 62–82.

[12] Haiyang Dai, Zhenping Chen, Renzhong Xue, Tao Li, Haizeng Liu, Yongqiang Wang, Structure and multiferroic properties of Eu-substituted BiFeO_3 ceramics, *Appl. Phys. A* 111 (2013) 907–912.

[13] P.C. Sati, M. Kumar, S. Chhoker, M. Jewariya, Influence of Eu substitution on structural, magnetic, optical and dielectric properties of BiFeO_3 multiferroic ceramics, *Ceram. Int.* 41 (2015) 2389–2398.

[14] R.D. Shannon, Revised effective ionic radii and systematic studies of interatomic distances in halides and chalcogenides, *Acta Crystallogr. A* 32 (1976) 751–767.

[15] T.D. Rao, R. Ranjith, S. Asthana, Enhanced magnetization and improved insulating character in Eu substituted BiFeO_3 , *J. Appl. Phys.* 115 (2014) 124110.

[16] A. Tamilselvan, S. Balakumar, M. Sakar, C. Nayek, P. Murugavel, K.K. Saravana, Role of oxygen vacancy and Fe–O–Fe bond angle in compositional, magnetic, and dielectric relaxation on Eu-substituted BiFeO_3 nanoparticles, *Dalton Trans.* 43 (2014) 5731–5738.

[17] V.R. Reddy, D. Kothari, A. Gupta, S.M. Gupta, Study of weak ferromagnetism in polycrystalline multiferroic Eu doped bismuth ferrite, *J. Appl. Phys. Lett.* 94 (2009) 082505.

[18] S.N. Kallaev, R.G. Mitorov, Z.M. Omarov, G.G. Gadzhiev, L.A. Reznichenko, Heat capacity of BiFeO_3 -based multiferroics, *J. Exp. Theor. Phys.* 118 (2014) 279–283.

[19] P. Uniyal, K.L. Yadav, Room temperature multiferroic properties of Eu doped BiFeO_3 , *J. Appl. Phys.* 105 (2009) 07D914.

[20] X. Zhang, Y. Sui, X. Wang, Y. Wang, Z. Wang, Effect of Eu substitution on the crystal structure and multiferroic properties of BiFeO_3 , *J. Alloys Compd.* 507 (2010) 157–161.

[21] D. Kothari, V.R. Reddy, A. Gupta, C. Meneghini, G. Aquilanti, Eu doping in multiferroic BiFeO_3 ceramics studied by Mossbauer and EXAFS spectroscopy, *J. Phys.: Condens. Matter* 22 (2010) 356001.

[22] I.I. Makoed, A.F. Revinskii, Specific features of the evolution of magnetic properties of bismuth ferrite modified with rare-earth element cations, *Phys. Solid State* 57 (2015) 1787–1792.

[23] V. Petříček, M. Dušek, L. Palatinus, Crystallographic computing system JANA2006: general features, *Cryst. Mater.* 229 (2014) 345–352.

[24] A.F. Ravinski, I.I. Makoed, K. Kokoshkevich, K.I. Yanushkevich, A.I. Galyas, V.V. Triguk, Magnetic properties and electron density distribution of $\text{La}_x\text{Bi}_{1-x}\text{FeO}_3$, *Inorg. Mater.* 43 (2007) 860–865.

[25] A.K. Singh, S.D. Kaushik, B. Kumar, P.K. Mishra, A. Venimadhav, V. Siruguri, S. Patnaik, Substantial magnetoelectric coupling near room temperature in $\text{Bi}_2\text{Fe}_4\text{O}_9$, *Appl. Phys. Lett.* 92 (2008) 132910.

[26] G. Alvarez, J. Contreras, A. Conde-Gallardo, H. Montiel, R. Zamorano, Detection of para-antiferromagnetic transition in $\text{Bi}_2\text{Fe}_4\text{O}_9$ powders by means of microwave absorption measurements, *J. Magn. Magn. Mater.* 348 (2013) 17–21.

[27] A.V. Pashchenko, V.P. Pashchenko, V.K. Prokopenko, V.A. Turchenko, Yu.F. Revenko, A.S. Mazur, V.Ya. Sycheva, N.A. Liedienov, V.G. Pitsyuga, G.G. Levchenko, Role of structure imperfection in the formation of the magnetotransport properties of rare-earth manganites with a perovskite structure, *J. Exp. Theor. Phys.* 124 (2017) 100–113.

[28] V.E. Dmitrienko, E.N. Ovchinnikova, S.P. Collins, G. Nisbet, G. Beutier, Y.O. Kvashnin, V.V. Mazurenko, A.I. Lichtenstein, M.I. Katsnelson, Measuring the Dzyaloshinskii-Moriya interaction in a weak ferromagnet, *Nat. Phys.* 10 (2014) 202–206.

[29] A.A. Amirov, I.I. Makoed, Y.A. Chaudhari, S.T. Bendre, D.M. Yusupov, A.Sh. Asvarov, N.A. Liedienov, A.V. Pashchenko, Magnetocaloric effect in $\text{BiFe}_{1-x}\text{Zn}_x\text{O}_3$ multiferroics, *J. Supercond. Nov. Magn.* 31 (2018) 3283–3288.

[30] T. Moriya, Anisotropic superexchange interaction and weak ferromagnetism, *Phys.*

- Rev. 120 (1960) 91–98.
- [31] A.K. Zvezdin, V.M. Matveev, A.A. Mukhin, A.I. Popov, Rare-earth ions in magnetically ordered crystals, *Solid-State Phys.* (1985) 296.
- [32] A. Bombik, B. Lesniewska, J. Mayer, A.W. Pacyna, Crystal structure of solid solutions $\text{REFe}_{1-x}(\text{Al or Ga})_x\text{O}_3$ (RE = Tb, Er, Tm) and the correlation between superexchange interaction $\text{Fe}^{+3}-\text{O}^{2-}-\text{Fe}^{+3}$ linkage angles and Neel temperature, *J. Magn. Mater.* 257 (2003) 206–219.
- [33] M.A. Hamad, Theoretical work on magnetocaloric effect in $\text{La}_{0.75}\text{Ca}_{0.25}\text{MnO}_3$, *J. Adv. Ceram.* 1 (2012) 290–295.
- [34] G.J. Song, G.J. Ma, J. Su, T.X. Wang, H.G. Yang, F.G. Chang, Effect of Ho^{3+} doping on the electric, dielectric, ferromagnetic properties and T_C of BiFeO_3 ceramics, *Ceram. Int.* 40 (2014) 3579–3587.
- [35] I. Levin, S. Karimi, V. Provenzano, C.L. Dennis, H. Wu, T. Comyn, J. Stevenson, I.S. Ronald, I.M. Reaney, Reorientation of magnetic dipoles at the anti-ferroelectric–paraelectric phase transition of $\text{Bi}_{1-x}\text{Nd}_x\text{FeO}_3$ ($0.15 \leq x \leq 0.25$), *Phys. Rev. B* 81 (2010) 020103(R).
- [36] P. Kumar, N. Shankhwar, A. Srinivasan, M. Kar, Oxygen octahedra distortion induced structural and magnetic phase transitions in $\text{Bi}_{1-x}\text{Ca}_x\text{Fe}_{1-x}\text{Mn}_x\text{O}_3$ ceramics, *J. App. Phys.* 117 (2015) 194103.
- [37] C. Ederer, C.J. Fennie, Electric-field switchable magnetization via the Dzyaloshinskii-Moriya interaction: FeTiO_3 versus BiFeO_3 , *J. Phys.: Condens. Matter* 20 (2008) 434219.